Proceedings of the 7th International Symposium on Cavitation
CAV2009 – Paper No. 139
August 17-22, 2009, Ann Arbor, Michigan, USA

Vorticity Confinement methods for cavitating flows

T. Hachmann
Institute of Fluid Dynamics and Ship Theory
Hamburg University of Technology, Germany

U. Lantermann
Institute of Fluid Dynamics and Ship Theory
Hamburg University of Technology, Germany

M. Abdel-Maksoud
Institute of Fluid Dynamics and Ship Theory
Hamburg University of Technology, Germany

D. Hänel
Institute of Combustion and Gas Dynamics
University Duisburg-Essen, Germany

ABSTRACT

Present work deals with investigations of numerical aspects of cavitating vortex dominated flows.

Computations of the viscous flow on realistic, technical configurations require efficient methods and high grid resolution, which is not sufficient in most cases to capture important details of the flow. Insufficient resolution increases the numerical dissipation of vortices generated at the tip region of lifting surfaces. One possible solution to reduce the unphysical decay of the strength of the vortices (despite of moderate resolution) is the application of vorticity confinement methods. Aim of the paper is the development and the comparison of Vorticity Confinement (VC) methods for cavitating flows on unstructured grids. Applications are proposed to control devices and marine propulsion systems.

The numerical dissipation of vortices is compared for different VC formulations. Especially the influence of the source terms on cavitating flows is investigated. The numerical computations are carried out by the finite volume solution method FreSCo on arbitrary grids. In the study vorticity confinement techniques are combined with different cavitation models available in the applied numerical method to investigate tip vortex flow. The cavitation models are based on Volume-of-Fluid (VoF). A NACA16020 elliptical wing is selected as a validation case. The combination of vorticity confinement formulations and cavitation models enables a better and a more detailed study of cavitation effects.

INTRODUCTION

Investigations of cavitating flows are of interest in many scientific and technical problems. Numerical simulations of cavitating flows with an Euler-Euler based cavitation approach have been performed in a number of studies [5,6,7] and showed satisfactory results. The computation effort for vortex dominated flows is still very high to reach similar results to experimental results. Numerical techniques to reduce vortex dissipation in non-highly resolved meshes have been performed and showed good results for different vortex dominated flows. [1,2,3]

Aim of the present paper is a critical analysis of existing cavitation models in combination with vorticity confinement methods in complex vortical flows. The need for studying the models in more detail results from the increased demond for numerous computations of technical problems in marine engineering. The usually used commercial codes based on Finite-Volume methods and Euler-Euler approaches perform sufficiently well for “smooth” problems, but show insufficient accuracy in more complex, stronger vortical flows.

The Euler-Euler approaches are based on a continuous vapour phase, defined by a volume fraction of vapour. The volume fraction is modelled by a transport equation with a source term. This concept is efficient and allows two-way coupling between flow and bubble phase, but it is not accurate enough as detailed studies have shown.

VORTICITY CONFINEMENT METHODS

The basic idea of Vorticity Confinement methods is to add anti-diffusive terms to the momentum equations of the fluid and was introduced by Steinhoff et. al. [1] in 1994. The momentum equation is

$$\frac{\partial \vec{v}}{\partial t} + (\vec{v} \cdot \nabla)\vec{v} = \frac{1}{\rho}\nabla p + \mu \nabla^2 \vec{v} - \varepsilon \vec{s} \qquad (1)$$

with the confinement term $\vec{s}$ and a control parameter ε.

The simplest form of the anti-diffusive source term is

$$\vec{s} = \rho \hat{n} \times \vec{\omega} \qquad (2)$$

with

$$\hat{n} = \frac{\nabla|\vec{\omega}|}{|\nabla|\vec{\omega}||} \tag{3}$$

pointing to the vortex core. While $\vec{n}$ gives the direction of the source term, the strength of the source term is calculated by the vorticity vectors as rotation of the velocity field.

$$\vec{\omega} = \nabla \times \vec{v} \tag{4}$$

The confinement parameter ε with the dimension of a velocity is kept as a constant and works fine on Cartesian or non-highly stretched grids. Numerical experiments on Cartesian grids with single and twin vortices have shown a remarkable improvement of vortex representation, which means lower dissipation of the vorticity strength.

For non-Cartesian grids Löhner & Yang [2] introduced a cell dependent dimensionless characteristic length in the direction of the gradient of the vorticity. To avoid numerical instabilities a switch was devised to deactivate vorticity confinement in boundary layers. By this extension the vorticity confinement model is more applicable to highly stretched grids. The calculations with the Löhner based formulation in this work were carried out with

$$\vec{s} = c_v \rho h^2 \nabla|\vec{\omega}| \times \vec{\omega} \tag{5}$$

and the following formulation for the local Reynolds-number:

$$\mathrm{Re}_{w,h} = \frac{\rho|\nabla|\vec{\omega}||h^3}{\mu} \tag{6}$$

Butsuntorn et. al. [3] proposed two new formulations. In the first formulation the confinement parameter is scaled with the velocity magnitude, the second formulation factors out of the first formulation and led to a confinement term directly proportional to the helicity. Butsuntorn et. al. [3] combined these ideas with a mesh dependency based on a non-directional cell volume formulation.

A sensitivity analysis with different grid resolutions and a Burgers vortex velocity profile as inlet boundary condition has shown good results for the helicity based formulation of Butsuntorn & Jameson.

$$\vec{s} = |\vec{u} \cdot \vec{\omega}| \cdot \left[1 + \log_{10}\left(1 + \frac{V}{V_{averaged}} \right)^{\frac{1}{3}} \right] \cdot \left(\rho \hat{n} \times \frac{\vec{\omega}}{|\vec{\omega}|} \right) \tag{7}$$

In case of highly stretched grids the non-directional cell volume formulation tends to an underestimation of the anti-dissipative source term. For this case a correction term subjected to a formulation of a cell aspect ratio was carried out by the sensitivity analysis and was added as follows.

$$\vec{s} = |\vec{u} \cdot \vec{\omega}| \cdot \left[1 + \log_{10}\left(1 + \frac{V}{V_{averaged}} \right)^{\frac{1}{3}} \right] \cdot \left(\rho \hat{n} \times \frac{\vec{\omega}}{|\vec{\omega}|} \right) \cdot \left[1 + \alpha \left(\frac{1}{n} \sum_{i=1}^{n} |l_i - l_{\min}| \right) \right] \tag{8}$$

with l as a length form the cell center to each face of the cell. The increase of the anti-dissipative source term causes nearly the same dissipation of the vortex on a Cartesian and on a highly stretched grid.

NUMERICAL METHODS

The Finite-Volume Navier-Stokes procedure FreSCo uses a segregated algorithm which is based on the strong conservation form of the momentum equation and employs a cell-centered, co-located storage arrangement for all transport properties [4]. The procedure can be used in conjunction with structured-grid and unstructured-grid discretisations, based on arbitrary polyhedral cells including cells with hanging nodes.

The implicit numerical approximation is second-order accurate in space and time. Integrals are approximated using the conventional mid-point rule. Diffusion terms are subsequently approximated using second-order central differences, whereas advective fluxes are approximated using high-order bounded (monotonic) schemes. The latter are applied in scalar form by means of a deferred correction approach.

Various turbulence-closure models are available with respect to statistical (RANS) approaches. Two phase flows are addressed by interface-capturing methods based upon the Level-Set or Volume-of-Fluid (VOF) technique. Fully conservative interface-sharpening techniques are optionally available.

Linear equations systems are solved by means of Krylov-subspace methods offered by the PETSC library. Since the date structure is generally unstructured, suitable preconditioned iterative sparsematrix solvers for symmetric and non-symmetric systems (e.g. GMRES, BiCG, QMR, CGS, BiCGStab) can be employed. The algorithm is parallelised using a domain-decomposition technique based on a Single Program Multiple Data (SPMD) message-passing model, i.e. each process runs the same program on its own subset of data. Inter-processor communication employs the MPI communications protocol. Load balancing is achieved using the ParMETIS partitioning software.

CAVITATION MODELLING

In the present study Vorticity Confinement is coupled with in the numerical method implemented cavitation models. In the Volume-of-Fluid (VoF) based cavitation models the fluid is considered as a binary mixture of a liquid and a gaseous phase. First one (index l) is the combination of water and the therein homogeneously distributed air. The second phase is the vapour (index v). The mixture density is the sum of the partial densities

$$\rho = \rho_l + \rho_v \tag{9}$$

Both, the liquid and the vapour phase, are modelled by Euler equations which lead to an Euler-Euler-Solution method. The vapour phase is represented by a volume fraction

$$\alpha = \frac{V_v}{V_v + V_l} \tag{10}$$

which is limited by $0 \le \alpha \le 1$. The mixture density is determined from the volume fraction by

$$\rho = \alpha\rho_v + (1-\alpha)\rho_l \tag{11}$$

The rate of change and the transport of α are described by an additional source term on the right hand side of the continuity equation. Three formulations of the source term by Singhal [5], Sauer [6] and Zwart [7] are used in this work.

The model by Singhal [5] is based on linear coherence between pressure and phase change. A phase change starts with the fall below the vapour pressure and increases with the raise of this pressure difference. The source term for evaporation and condensation are as follows:

$$s = (R_e + R_c)\cdot\Delta p \text{ with} \tag{12}$$

$$R_e = C_e \cdot \frac{\rho_l}{\rho_v} \cdot \frac{1}{p_\infty t_\infty} \cdot \alpha \text{ if } \Delta p > 0 \text{ and} \tag{13}$$

$$R_c = C_c \cdot \frac{1}{p_\infty t_\infty} \cdot (1-\alpha) \text{ if } \Delta p < 0 \tag{14}$$

C_e and C_c are empirical constants (C_e=80.0, C_c=1.0) and

$$t_\infty = \frac{l_{ref}}{v_\infty} \tag{15}$$

The model by Sauer [5] is based on the Rayleigh-Plesset-Equation. The Rayleigh-Plesset equation models the growth and decay of vapour spherical bubbles. The cavitation starts from a nuclei, modelled as micro bubbles with a prescribed initial radius R_0. When a nucleus reaches a region below vapour pressure it begins to growth caused by vaporization.

$$R\ddot{R} + \frac{3}{2}\dot{R}^2 = \frac{1}{\rho}\left[p_v + p_{g0}\left(\frac{R_0}{R}\right)^{3k} - p_\infty - \frac{2\sigma}{R} - \frac{4\mu\dot{R}}{R} + \frac{\rho}{4}(\vec{v} - \vec{v}_B)^2 \right]. \tag{16}$$

Here σ is the surface tension, p_{g0} is the initial pressure of the non-condensable gas inside the bubble, k is the isentropic exponent and p_∞ is the local fluid pressure.

If the acceleration of the radius $\ddot{R}$ is assumed to be small and if viscosity and surface tension are insignificant, the nonlinear differential equation Eq. (16) reduces to the algebraic equation which is used in this model.

$$\dot{R} = \sqrt{\frac{2}{3}\frac{p_v - p_\infty}{\rho}}. \tag{17}$$

The vapour phase is an accumulation of a number of single bubbles and leads to a nonlinear coherence between pressure and phase change. The source term is formed as follows:

$$s = \left[\frac{3\alpha}{R_b} \cdot \frac{1}{\sqrt{\rho_l |\Delta p|}} \right] \cdot \Delta p \tag{18}$$

The model by Zwart [7] is a further development of the model by Sauer and introduces the fusion of small bubbles. The source term for evaporation and condensation are as follows:

$$s = (R_e + R_c)\cdot\Delta p \text{ with} \tag{19}$$

$$R_e = F_{vap} \cdot \frac{3 r_{nuc}(1-\alpha)\rho_v}{R_B} \sqrt{\frac{2}{3}\frac{p_v - p}{\rho_l}} \text{ if } p < p_v \text{ and} \tag{20}$$

$$R_c = F_{cond} \cdot \frac{3\alpha\rho_v}{R_B} \sqrt{\frac{2}{3}\frac{p - p_v}{\rho_l}} \text{ if } p > p_v \tag{21}$$

All of the Euler-Euler-approaches result in a two-way coupled system of equations. The system is then solved by Finite-Volume- of Finite-Element-Methods. The main disadvantage is the restriction to simplified bubble dynamics in the Euler representation of the bubble phase

RESULTS

CASE 1: Single vortex

The first combination of Vorticity Confinement methods with Euler-Euler based cavitation models were carried out with a single vortex in an undisturbed flow. The velocity profile of an initial Burgers Vortex is given as follows

$$v_\varphi = \frac{\Gamma}{2\pi r} \cdot \left(1 - e^{-1{,}256\frac{r^2}{a^2}} \right) \tag{22}$$

where r is the radius, a is the core radius of the vortex and Γ is the circulation. These velocity conditions are added as inlet boundary conditions in a cylindrical domain with free slip wall boundary conditions and a pressure boundary condition at the outlet. The used computational grid has approx. 200000 hexahedral cells. The vortex region has uniform cells and approx. uniform cells are located next to the wall boundary of the calculation domain. The flow is considered to be laminar. The topology and grid of this test case can be seen in figure. 1

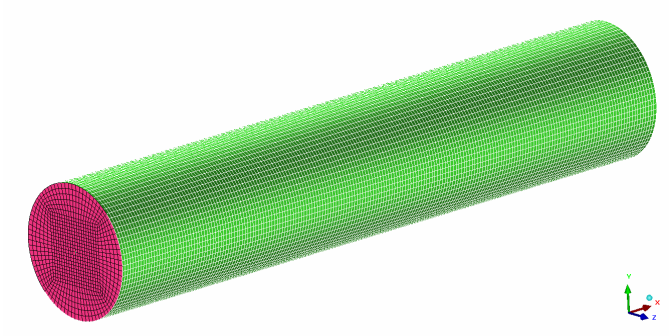

Figure 1: Topology and computational grid for calculation with Burgers-Vortex-model

The vapor volume fraction of a single cavitating vortex with and without Vorticity Confinement is shown in figure 2.

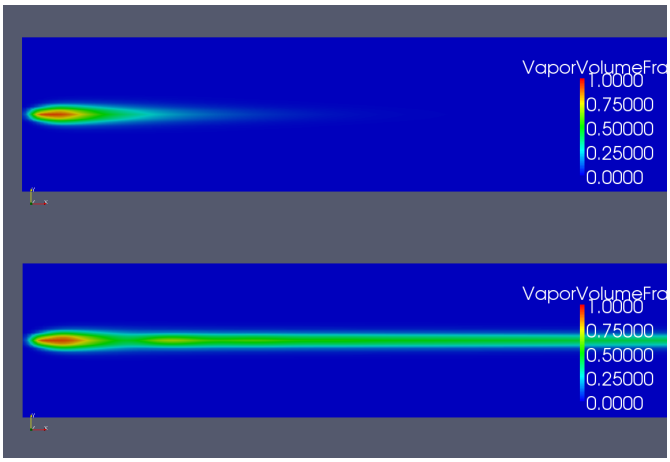

Figure 2: Vapor volume fraction for Burgers-Vortex with and without Vorticity-Confinement

As expected, the vapor fraction decreases rapidly in the basic calculation while the vapor volume fraction is noticeably elongated in the calculation with Vorticity Confinement. In this case the helicity based formulation with a confinement parameter $\varepsilon = 0{,}01$ is used.

The effect of the elongation of the vapour phase is of course dependent on the confinement parameter ε. Too large values of ε do not only cause unphysical results but also tend to introduce numerical instabilities. To avoid these numerical instabilities an automatic adaption of ε is implemented. The calculation starts with a low ε. The value of ε increases gradually during the calculation in dependency of the residuals. This technique is also used for the following NACA 16020. This leads to a higher value ε and less vortex dissipation.

CASE 2: Tip vortex of a NACA 16020 wing

To estimate the quality of the prediction of cavitation in tip vortices computations were carried out for a submerged hydrofoil in 3-D. That is the configuration investigated by Fruman et. al. [8]. The experiments of the elliptical hydrofoil of area ratio 3.8 and identical NACA16020 cross sections with a chord length of 80mm and an angle of attack of 10°. The experiment tests were carried out at the Ecole Navale cavitation tunnel in Lanveoc. The dimension of the computation domain is equivalent to the dimensions of the cavitation tunnel with a 1m long test section and a square section of 192mm. An overview of the computation domain and the surface grid can be seen in figure 3 and 4.

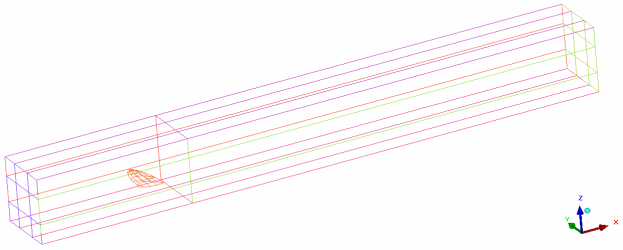

Figure 3: Topology of the test section in the ENCT cavitation tunnel

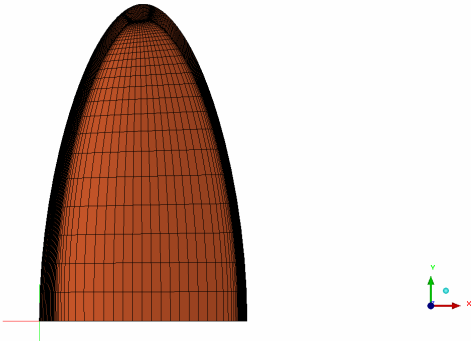

Figure 4: Surface grid of the NACA16020 elliptical wing

The hydrofoil is mounted horizontally on one of the vertical walls of the 192mm sides at 300mm from the inlet. Two Reynolds numbers were considered: Re=1.2e6 for validation computations of the lift coefficient and Re=1.08e6 for tangential tip vortex velocity profiles. The Reynolds number is based on the chord length c. For validation of the computation results the lift coefficient is available for the Re=1,2e6 and the tangential tip vortex velocity profiles for Re=1,08e6. The effects of turbulence were modelled with the k-ω turbulence model with a given free stream turbulence of 1.5%. At the inlet a velocity is defined according to the Reynolds number. The boundary condition at the outlet is a pressure boundary condition prescribing hydrostatic pressure. Wall boundary condition is applied to the hydrofoil and the tunnel walls.

Two numerical grids have been applied. The first one has 750000 control volumes and the second one 2.9 Millions. The vorticity confinement models were tested on the coarse grid. The results of the fine grid are used to evaluate the performance of the different vorticity confinement formulations. The block structured hexahedral grid has an O-Grid topology around the hydrofoil and was generated by using ICEM-CFD. In the following text the Vorticity Confinement formulation by Löhner et. al. is marked as VC1, the first formulation of

Butsuntorn et. al. is marked as VC2 and the helicity based formulation by Butsuntorn et. al. is marked as VC3.

The calculated lift coefficients for Re=1.2e6 agree well with the experimental estimated value of c_l=0,3 especially the results of Singhal cavitation model [8] with a difference of less than 3%. For the Sauer and Zwart model the mesh density at the root section of the wing is insufficient to simulate the vapor phase correctly. The vapor phase in this area is too small and results in a higher lift coefficient.

The calculated lift and drag coefficients for Re=1.08e5 are plotted in figure 5 and 6. The measured lift coefficients is c_l=0,4 and the measured drag coefficient is approx. c_d=0,04. With the exception of the VC2 formulation a light increase of the lift coefficient is determined. The VC2 formulation shows an increase of the lift coefficient by approximately 10% in comparison with the results of Sauer and Zwart model. Also for the drag coefficient the VC2 formulation tends to an overestimation. Especially in combination with the Sauer model c_d increases by more than 20%. The lowest influence on lift and drag coefficient appeared with the VC3 model.

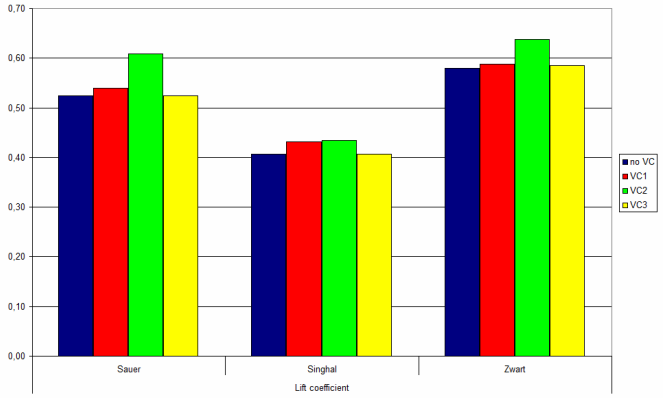

Figure 5: Lift coefficient for Re=1.08e6, three different cavitation models and three different Vorticity Confinement formulations

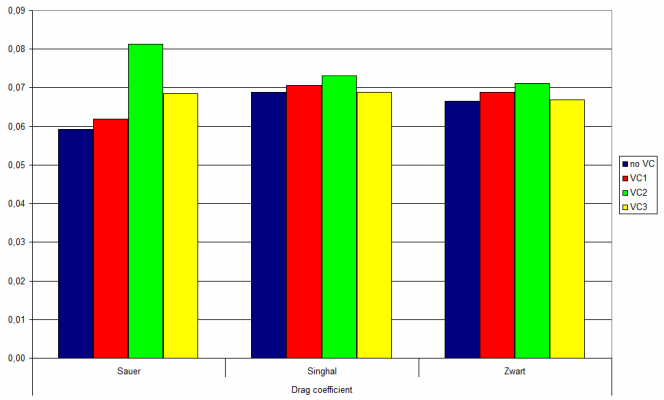

Figure 6: Drag coefficient for Re=1.08e6, three different cavitation models and three different Vorticity Confinement formulations

The following figure format is similar to the one Fruman et. al. [7] used in their paper to publish experimental results. The vertical component of the velocity at the tip vortex region is plotted at different stations behind the wing tip. The tangential velocities are normalized by the freestream velocity v_{oo}. Results are shown for the helicity based vorticity confinement formulation (VC3). The VC2 formulation shows in comparison to the VC3 formulation for this setup lower vortex dissipation but significant increase of c_l and c_d. As consequence this formulation is not considered in the further evaluation. Figure 7 shows the influence of the different vorticity confinement methods on the tangential velocity at the station y/c_{max}=0,750 in combination with the Sauer cavitation model.

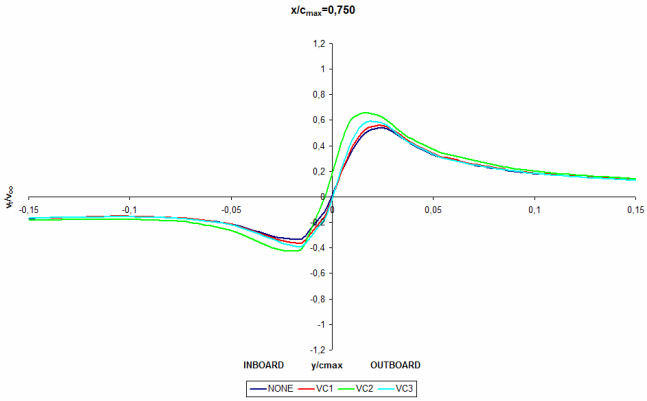

Figure 7: Tangential velocities as a function of distance to the vortex center at station x/c_{max}=0,075

The VC3 formulation showed similar results to the VC1 formulation for c_l and c_d although the VC1 formulation includes the exclusion of the boundary layer for the vorticity confinement source terms. Beside the lowest influence on lift and drag coefficients the performance of the different cavitation models in combination with the VC3 in this setup can be evaluated by focusing a detailed view of the tangential velocities in comparison to a high resolution mesh with 2,9 Mio. hexahedral cells. The values of ε vary from ε=0,05 for the Sauer model to ε=0,026 for the Singhal model and to ε=0,017 for the Zwart model.

The tangential velocity distribution at x/c_{max}=0.500 is presented in figure 8. It directly shows the flow around the wing tip. Compared to the experimental results the prediction of the tangential velocities of all models is higher than in the experiment. The lowest amount can be found for the results of Singhal cavitation model. This model has the lowest c_l and therefore the lowest circulation at the wing tip.

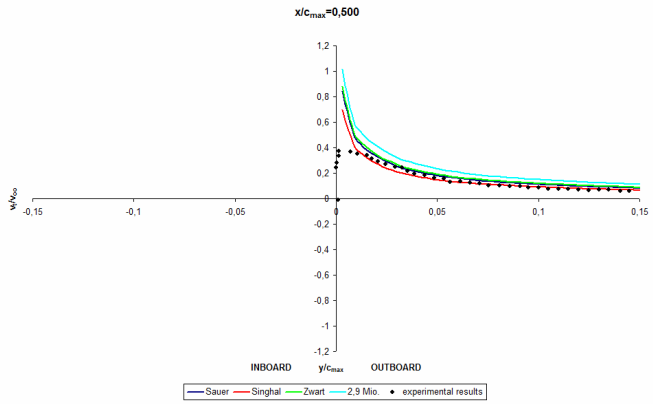

Figure 8: Tangential velocities as a function of distance to the vortex center at station x/c_{max}=0,500

Figure 9 shows the tangential velocities at x/c_{max}=0,550. This is the station where a flow directed from the suction to the pressure side can first be found on the inboard side. The tangential velocity profile is similar to the vortex model used in case 1. The maximal tangential velocity at the outboard side is higher for the Sauer and Zwart model than at the wing tip (x/c_{max}=0,500) which is in accordance to the experimental results. For all models, especially for the high mesh resolution, the maximum velocity is still overpredicted in comparison to the experimental results.

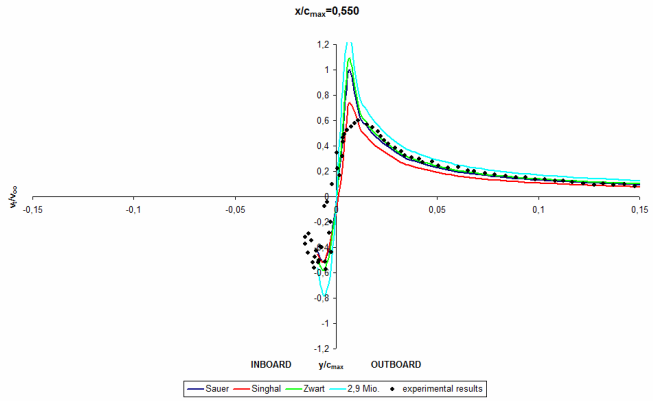

Figure 9: Tangential velocities as a function of distance to the vortex core at station x/c_{max}=0,550

Figure 10 again shows tangential velocity profiles of the wing tip vortex. At the station x/c_{max}=0,625 the velocity gradient at the vortex center decreases and the vortex core radius increases. This is in accordance to the experimental results for all cavitation models. A slight difference can be seen for the Singhal model and for the fine mesh results. The vortex center of the Sauer and Zwart model stayed straight behind the wing tip while for the Singhal model the vortex core moved to the outboard side. The vortex center of the fine grid moved to the inboard side.

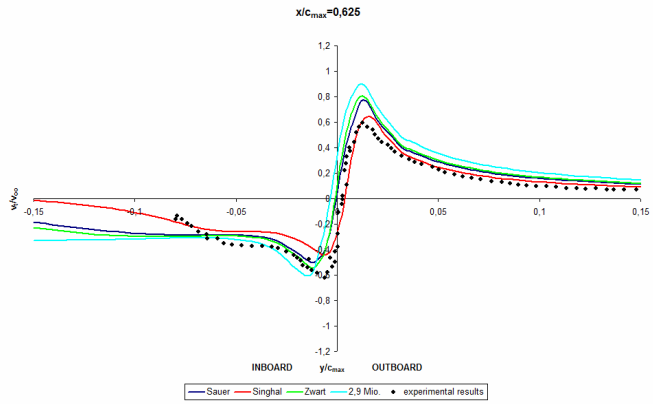

Figure 10: Tangential velocities as a function of distance to the vortex core at station x/c_{max}=0,625

At the station x/c_{max}=0,750 (figure 11) the vortex radius continues to expand for all calculations and the tangential velocity profiles are loosing their sharp maximum and minimum while the maximum velocities for the Sauer and Zwart model are slightly lower than in the experiment. The vortex center for the Singhal model moved further to the outboard side and the vortex center for the high resolved mesh further to the inboard side.

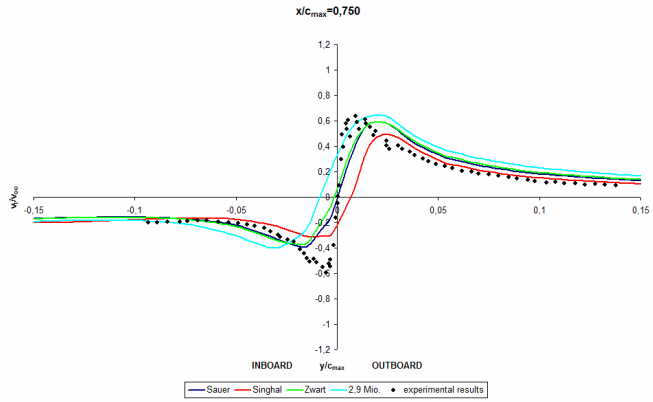

Figure 11: Tangential velocities as a function of distance to the vortex core at station x/c_{max}=0,750

For station x/c_{max}=1,000 (figure 12) the calculated absolute values of the tangential velocity decreased to approx. v/v_{oo}=0,4. The vortex core radius expands to approx. x/c_{max}=0,025. The maximum and minimum velocities and the vortex core radius are not in accordance to the experimental results. Velocities of more than v/v_{oo}=0,6 and a core radius of approx. x/c_{max}=0,01 are measured in the ENCT cavitation tunnel. Actually the highly resolved mesh showed similar results as the coarse grid with confinement techniques.

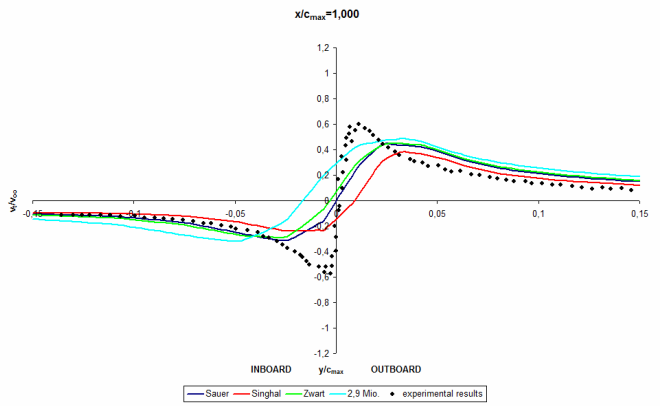

Figure 12: Tagential velocities as a function of distance to the vortex core ate station x/c_{max}=1,000

CONCLUSION

Numerical investigations of different cavitation models for cavitating two-phase flows were performed in combination with different vorticity confinement formulations. The different Euler-Euler approach based cavitation models and vorticity confinement techniques, inclusive widely used simplifications, are presented. Comparisons for different test cases have shown that the combination of Euler-Euler cavitation modelling and vorticity confinement techniques work together. The influence of the vorticity confinement source terms on the lift and drag coefficient is for most of the presented techniques neglectable. With the combination of vorticity confinement techniques and cavitation models it is possible to simulate tip vortices with the same accuracy at a lower number of cells in comparison to a higher mesh resolution. However, to simulate cavitating tip vortices these techniques are not sufficient. The dissipation of vorticity in the core region can be reduced with vorticity confinement techniques to reach values which are similar to the results of computations with higher mesh resolution but the vortex core radius tends to increase. Possible ways to reach the accuracy of experimental results are to use local refinement methods or overlapping grids technology in combination with vorticity confinement techniques in vortex core regions with high vorticity gradients.

NOMENCLATURE

a	core radius [m]
c_{max}	maximum hydrofoil chord length [m]
C_c	empirical constant [-]
c_d	drag coefficient [-]
C_e	empirical constant [-]
c_l	lift coefficient [-]
c_v	confinement parameter [-]
F_{cond}	empirical constant [-]
F_{vap}	empirical constant [-]
h	length scale [m]
k	isentropic exponent [-]
l_{ref}	reference length [-]
p	pressure [Pa]
p_{G0}	initial pressure inside the bubble [Pa]
p_{oo}	local pressure [Pa]
$\vec{s}$	source [m/s^2]
$\hat{n}$	vector pointing to vortex center [-]
l_i	length scale [m]
l_{min}	minimum length scale [m]
r	radius [m]
r_{nuc}	empirical constant [-]
R_0	initial bubble radius [m]
R_B	bubble radius [m]
R_c	source term for condensation
R_e	source term for evaporation
Re	Reynolds number [-]
$Re_{\omega,h}$	local Reynolds number [-]
t_{oo}	constant time [s]
v_{oo}	local velocity [m/s]
V	volume [m^3]
$V_{averaged}$	average volume [m^3]
R	bubble radius [m]
t	time [s]
$\vec{v}$	fluid velocity [m/s]
$\vec{v}_B$	bubble velocity [m/s]
$\vec{v}_\varphi$	tangential velocity [m/s]
V_v	volume of vapor phase [m^3]
V_l	volume of liquid phase [m^3]
α	volume fraction of the vapor [-]
Γ	circulation [m^2/s]
ε	confinement parameter
μ	dynamic viscosity [kg/ms]
ρ	mixture density [kg/m^3]
ρ_l	density of the liquid phase [kg/m^3]
ρ_v	density of the vapor phase [kg/m^3]
σ	surface tension of the fluid [N/m]
$\vec{\omega}$	vorticity [1/s]

REFERENCES

[1] Steinhoff, 1994, "Vorticity Confinement: A New Technique for Computing Vortex Dominated Flows," pp. 235-263 in Frontiers of Computational Fluid Dynamics, J. Wiley & Sons 1994.

[2] Löhner, Yang 2001, "Tracking Vortices over Large Distances using Vorticity Confinement," ECCOMAS CFD 2001, Swansea, Wales.

[3] Butsuntorn, Jameson, 2008, "Time Spectral Method for Rotorcraft Flow with Vorticity Confinement," AIAA 2008-7340.

[4] Schmode, D., Rung,T, 2007, "RANS Code Verification Using Method of Manufactured Solution", 10th Numerical Towing Tank Symposium, Hamburg, Germany.

[5] Singhal, "Mathematical Basis and Validation of the Full Cavitation Model," Journal of Fluids Engineering, September 2002, Vol. 124

[6] Sauer, „Instationär kavitierende Strömungen - Ein neues Modell basierend auf Front-Capturing (VoF) und

Blasendynamik," Dissertation Universität Karlsruhe (TU), 2000

[7] Zwart, "A Two Phase Flow Model for Predicting Cavitation Dynamics," ICMF 2004, International Conference on Multiphase Flow, Yokohama, Japan

[8] Fruman, Dugué, Pauchet, Cerruti, Briançon-Marjolet, "Tip Vortex Roll-Up and Cavitation," 19th Symposium on Naval Hydrodynamics 1992, Seoul, Korea

[9] Vorhölter, Schmode, Rung, "Implementation of Cavitation Modelling in FreSCO," 9th Numerical Towing Tank Symposium, Le Croisic, France